Weak fountains in a stratified fluid

Wenxian Lin* and S. W. Armfield†
School of Aerospace, Mechanical and Mechatronic Engineering, University of Sydney, Sydney, NSW 2006, Australia
(Received 3 February 2002; revised manuscript received 16 August 2002; published 26 December 2002)

The behavior of weak axisymmetric and plane fountains resulting from the injection of denser fluid upwards into large containers containing a stably stratified fluid has been explored using dimensional analysis, scaling analysis, and direct numerical simulation. For weak fountains, with Froude number Fr ≈ 1.0, dimensional and scaling analyses have been used to derive scaling relations for the dimensionless fountain height, width, thickness of the temperature layer, and development times in terms of the Froude number Fr, Reynolds number Re, Prandtl number Pr, and ambient stratification number *s*. Numerical simulations have been carried out for a series of Fr, Re, Pr, and *s* for both axisymmetric and plane fountains to validate and quantify the scaling relations obtained by the dimensional and scaling analyses. The numerical results have been found to agree well with the analytical scaling relations.

DOI: 10.1103/PhysRevE.66.066308 PACS number(s): 47.27.Wg, 47.55.Hd, 47.60.+i

I. INTRODUCTION

Fountains occur with jets when the buoyancy force acting on the jet, as a result of a density difference between the jet fluid and the surrounding ambient fluid, acts in the opposite direction to that of the jet flow. Thus, both dense jets projected upwards into a less dense medium, and less dense jets projected downwards into a more dense medium, will produce fountains. Considering only the upward projected dense flow, the jet will penetrate to a finite height, with the fluid then falling back as a plunging plume. In cases where the jet source lies on a solid boundary and the ambient fluid is homogeneous, the plunging plume falls to the boundary and then forms a gravity intrusion traveling away from the main fountain flow.

The behavior of a fountain is mainly controlled by the Reynolds number Re, the Prandtl number Pr, and the Froude number Fr, which are defined as follows:

$$\mathrm{Re}=\frac{V_0 X_0}{\nu},\quad \mathrm{Pr}=\frac{\nu}{\kappa},\quad \mathrm{Fr}=\left(\frac{M_0 V_0}{B_0 X_0}\right)^{1/2}, \tag{1}$$

where V_0 is the discharge velocity, X_0 is the radius of the source orifice for an axisymmetric fountain or the half-width of the source slot for a plane fountain, ν and κ are the kinematic viscosity and thermal diffusivity of the fluid, M_0 and B_0 are the specific momentum and buoyant flux, respectively. When the discharge velocity at the source is uniform, M_0 and B_0 are obtained as

$$M_0=\pi V_0^2 X_0^2,\quad B_0=\pi g' V_0 X_0^2, \tag{2}$$

for axisymmetric fountains and

$$M_0=2V_0^2 X_0,\quad B_0=2g' V_0 X_0, \tag{3}$$

for plane fountains, where g' is the reduced gravity between the fountain and the ambient fluid at the discharge source. Therefore, for a uniform discharge velocity at the source, Fr is obtained for both axisymmetric and plane fountains as follows:

$$\mathrm{Fr}=\frac{V_0}{(X_0 g')^{1/2}}. \tag{4}$$

For strong fountains, the flow becomes turbulent quite close to the source, and such flows are characterized by Fr $\gg 1.0$. For these strong fountains, the fountain front, the plunging plume, and the intrusion flow are the distinct features. Many analytical and experimental studies on the fountain front and plunging plume have been carried out [1–12]. The fountain outflow forms a gravity intrusion similar to those that have been widely studied in other contexts [13–15]. In general, the fountain investigations have focused on the fountain front and plunging flow rather than the intrusion.

Weak fountains, characterized by Fr $\leqslant 1.0$, have some different patterns of behavior from those of strong fountains. Weak fountains have no distinguishable upward and downward flow, instead the streamlines curve and spread from the source. In particular, the fountain top, downflow plume, and intrusion are not distinct features, and the intrusion height is a substantial component of the total fountain height [16–19]. Such weak fountains are expected to be laminar. Earlier work has shown that the laminar scalings break down for Fr greater than ≈ 1.5 [17].

Weak fountains discharged into a stably stratified fluid have many applications. One example is the replenishing of cold salt water in solar ponds by weak fountain flows to maintain stable concentration and temperature gradients in order to suppress convective flows inside the ponds for the maximum collection and storage of solar energy [20]. A good understanding of the behavior of weak fountains in stratified fluids is essential for the design and management of these processes, as well as being of fundamental interest to fluid mechanics and heat transfer. Recently, we carried out a series of scaling analysis and numerical studies on the behavior of weak fountains in homogeneous fluids [16–19], however, no

*Electronic address: wenxian.lin@aeromech.usyd.edu.au
†Electronic address: armfield@aeromech.usyd.edu.au

 ©2002 The American Physical Society

study has been found that investigates the behavior of weak fountains in stratified fluids, which motivates us to conduct the current study.

Both scaling analysis and numerical simulations [16–19] showed that the dimensionless fountain height y_m and width x_w (nondimensionalized by X_0) provide a full parametrization of the fountain flow in the fountain core for weak fountains in a homogeneous ambient fluid. The vertical velocity and temperature on the symmetry axis were scaled with y_m and the horizontal distribution of both the vertical and horizontal velocities in the zone of self-similarity in the fountain core were scaled with both y_m and x_w. In addition, the dimensionless thickness Δy_T (nondimensionalized by X_0) of the temperature layer on the symmetry axis, over which the fountain fluid temperature changes from the inlet value to that of the ambient fluid, provides a parametrization of the thermal structure of the fountain front, and the dimensionless τ_{ms} and τ_{mf} (nondimensionalized by X_0/V_0) provide the time scales for the fountain flow in the fountain core to reach a steady state and for the temperature layer to achieve full development, respectively.

The primary purpose of this study is to obtain scaling relations describing the behavior of weak fountains with Fr $\leqslant 1.0$ when they are discharged into stably stratified ambient fluids. An initial scaling is obtained using dimensional arguments and assuming a power law relation between the fountain flow quantities and the control parameters. This approach cannot provide a complete description of the scaling for the case when viscosity is assumed important and the stratification of the ambient fluid has to be taken into account, as then the number of control parameters is greater than the number of dimensions, but does provide an indication of the correct scaling relation, requiring only the evaluation of two powers. To obtain tentative values for the unknown powers, a further scaling analysis is carried out based on the assumed viscous interaction that will influence the fountain height. The two flow regions, in which a viscous interaction will occur, are between the rising flow of the fountain core, and the downward outer flow, and within the viscous intrusion that forms downstream of the downward outer flow. Viscous interaction between the fountain core and downward outer flow will lead to a reduction in the fountain height, however, initial results showed that the fountain height increased with increasing viscosity so it was unlikely that this was the dominant viscous interaction in the flow. Increased viscous interaction in the intrusion means that either the intrusion height will increase, or that the horizontal pressure gradient that drives the intrusion will increase to balance the increased viscous force and maintain the same intrusion height. An increased intrusion height will require an increased fountain height for Fr<1.0, while an increased horizontal pressure gradient will also require an increased fountain height. Thus, the observed behavior of the weak fountain indicated that the primary viscous interaction was that occurring in the intrusion. This observation was used to construct a scaling relation and obtain tentative values for the unknown powers remaining in the relation obtained from a dimensional analysis. The scaling relations are validated using the numerical results and shown to provide a good prediction of the observed fountain behavior.

II. DIMENSIONAL AND SCALING ANALYSES

Under consideration are axisymmetric and plane fountains in a stably stratified fluid. In the case of the axisymmetric fountains, the physical system is a vertical cylindrical container of height H and radius L while in the case of the plane fountains, it is a rectangular container of height H and half-width L. In both the cases, the Newtonian fluid is initially at rest and linearly stratified, characterized by a constant stratification parameter S_p, with

$$S_p=\left[-\frac{1}{\rho_a(0)}\frac{d\rho_a(Y)}{dY}\right], \tag{5}$$

where $\rho_a(Y)$ and $\rho_a(0)$ are, respectively, the density of the ambient fluid at height Y and at $Y=0$, that is, the bottom of the container. The temperature stratification parameter is

$$S=\frac{\partial T_a(Y)}{\partial Y}=\beta S_p,$$

where $T_a(Y)$ is the temperature of the ambient fluid at height Y and β is the coefficient of thermal expansion of the fluid. The sidewall is nonslip and insulated and the top is open. On the bottom center, an orifice of radius X_0 for axisymmetric fountains or a slot of half-width X_0 for plane fountains is used for the fountain source. The remaining bottom region is a rigid nonslip insulated boundary. At time $t=0$, a stream of fluid with a uniform discharge velocity V_0 and at a lower temperature T_0 [$T_0<T_a(0)$] is discharged impulsively into the container from the source to initiate the fountain, and this discharge is maintained thereafter. For axisymmetric fountains, the flow is assumed to be axisymmetric and two dimensional while for plane fountains, the length in the spanwise coordinate is assumed to be long enough so that two-dimensional flow may be assumed.

For weak fountains discharged into a homogeneous fluid, it was shown that their behavior is well described by the fountain height Y_m, fountain width X_w, and time t_m for the flows in the fountain core to reach a steady state [16–19]. Additionally, ΔY_T, the thickness of the axis, over which the temperature changes from T_0 to $T_a(0)$, as shown in Fig. 1, where both the temperature and vertical velocity profiles on the axis at a steady state are sketched for weak fountains in a stratified fluid, provides a parametrization of the thermal structure of the fountain front. In a stratified fluid, S is an additional control variable apart from Re, Pr, and Fr. In the following dimensional and scaling analyses and the subsequent numerical simulations, only weak fountains with Fr ≈ 1.0 will be considered.

A. Governing equations

Due to the symmetry of the system geometry and the boundary and initial conditions, one-half of the physical domain may be chosen as the computational domain, while the weak fountain discharge makes it appropriate to assume a laminar flow. With the Boussinesq assumption, the governing

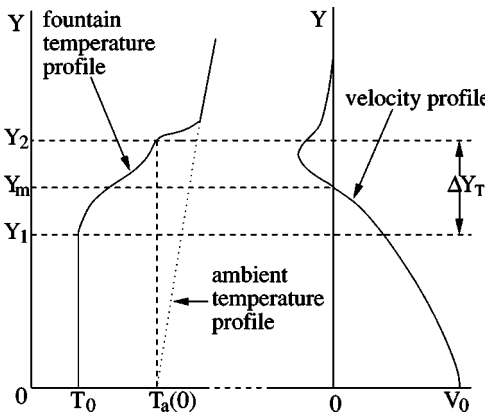

FIG. 1. A sketch of the profiles of the temperature and vertical velocity on the symmetry axis at a steady state.

equations are the Navier-Stokes equations and the temperature equation, which are written in dimensionless and incompressible form as follows:

$$\frac{1}{x^j}\frac{\partial(x^j u)}{\partial x}+\frac{\partial v}{\partial y}=0, \tag{6}$$

$$\frac{\partial u}{\partial \tau}+\frac{1}{x^j}\frac{\partial(x^j uu)}{\partial x}+\frac{\partial(vu)}{\partial y} =-\frac{\partial p}{\partial x}+\frac{1}{\mathrm{Re}}\left\{\frac{\partial}{\partial x}\left[\frac{1}{x^j}\frac{\partial(x^j u)}{\partial x}\right]+\frac{\partial^2 u}{\partial y^2}\right\}, \tag{7}$$

$$\frac{\partial v}{\partial \tau}+\frac{1}{x^j}\frac{\partial(x^j uv)}{\partial x}+\frac{\partial(vv)}{\partial y} =-\frac{\partial p}{\partial y}+\frac{1}{\mathrm{Re}}\left[\frac{1}{x^j}\frac{\partial}{\partial x}\left(x^j\frac{\partial v}{\partial x}\right)+\frac{\partial^2 v}{\partial y^2}\right]+\frac{1}{\mathrm{Fr}^2}(\theta-\theta_{b,y}), \tag{8}$$

$$\frac{\partial \theta}{\partial \tau}+\frac{1}{x^j}\frac{\partial(x^j u\theta)}{\partial x}+\frac{\partial(v\theta)}{\partial y}=\frac{1}{\mathrm{Re}\,\mathrm{Pr}}\left[\frac{1}{x^j}\frac{\partial}{\partial x}\left(x^j\frac{\partial \theta}{\partial x}\right)+\frac{\partial^2 \theta}{\partial y^2}\right], \tag{9}$$

where $j=0$ and 1 denote the plane fountains and axisymmetric fountains, respectively; x, y, u, v, τ, p, and θ are, respectively the dimensionless horizontal and vertical coordinates, x velocity and y velocity, time, pressure, and temperature. $\theta_{b,y}$ is the dimensionless temperature of the ambient fluid at height y.

Nondimensional quantities are obtained as follows:

$$x=\frac{X}{X_0},\quad y=\frac{Y}{X_0},\quad u=\frac{U}{V_0},\quad v=\frac{V}{V_0},$$

$$\tau=\frac{t}{(X_0/V_0)},\quad p=\frac{P}{\rho V_0^2},\quad \theta=\frac{T-T_{a,0}}{T_0-T_{a,0}}, \tag{10}$$

where ρ is density and X, Y, U, V, t, P, and T are the corresponding dimensional quantities.

The appropriate initial and boundary conditions are

$$u=v=0,\quad \theta=\theta_{b,y},\quad \text{at all } x,y, \tag{11}$$

when $\tau<0$ and

$$u=0,\quad \frac{\partial v}{\partial x}=0,\quad \frac{\partial \theta}{\partial x}=0\quad \text{at } x=0,\quad 0\leqslant y\leqslant\frac{H}{X_0};$$

$$u=v=0,\quad \frac{\partial \theta}{\partial x}=0\quad \text{at } x=\frac{L}{X_0},\quad 0\leqslant y\leqslant\frac{H}{X_0};$$

$$u=0,\quad v=1,\quad \theta=1\quad \text{at}\quad 0\leqslant x\leqslant 1,\quad y=0;$$

$$u=v=0,\quad \frac{\partial \theta}{\partial y}=0\quad \text{at}\quad 1<x\leqslant\frac{L}{X_0},\quad y=0;$$

$$\frac{\partial u}{\partial y}=\frac{\partial v}{\partial y}=0,\quad \frac{\partial \theta}{\partial y}=s\quad \text{at}\quad 0\leqslant x\leqslant\frac{L}{X_0},\quad y=\frac{H}{X_0}, \tag{12}$$

when $\tau\geqslant 0$.

B. Scaling relations

1. Fountain height

As Fr is ≈ 1.0, both the specific momentum flux M_0 and the specific buoyancy flux B_0 are important. For weak fountains considered here, the kinematic viscosity ν is also important, together with the stratification S_p when the ambient is stratified. These four parameters will provide a complete parametrization of the fountain height Y_m, which is defined as the height, at which the vertical velocity of the fountain front on the symmetry axis is zero at a steady state, as shown in Fig. 1. Expressing Y_m in terms of M_0, B_0, S_p, and ν as

$$Y_m[=]M_0^a B_0^b S_p^c \nu^d, \tag{13}$$

where "[=]" means "has the dimension of."

For axisymmetric fountains, M_0, B_0, S_p, and ν have the following units:

$$M_0[=]L^4T^{-2},\quad B_0[=]L^4T^{-3},$$

$$S_p[=]L^{-1},\quad \nu[=]L^2T^{-1}, \tag{14}$$

where L and T represent the dimensions of length and time, respectively. Therefore, from Eq. (13), we have

$$L[=](L^4T^{-2})^a(L^4T^{-3})^b(L^{-1})^c(L^2T^{-1})^d$$
$$[=]L^{(4a+4b-c+2d)}T^{(-2a-3b-d)}. \tag{15}$$

Hence, dimensional consistency then requires

$$4a+4b-c+2d=1, \tag{16}$$

$$-2a-3b-d=0, \tag{17}$$

which give the following relations:

$$a=-\frac{d}{2}+\frac{3}{4}(1+c), \quad b=-\frac{1}{2}(1+c). \tag{18}$$

With these relations, we find that for axisymmetric fountains,

$$Y_m[=]\pi^{-(1/2)(1+c+d)}[\beta(T_0-T_{a,0})]^c \mathrm{Fr}^{(1+c)} s^c \mathrm{Re}^{-d} X_0 \sim \mathrm{Fr}^{(1+c)} s^c \mathrm{Re}^{-d} X_0, \tag{19}$$

where "$\sim$" means "scales with," $\pi^{-(1/2)(1+c+d)}[\beta(T_0-T_{a,0})]^c$ is a dimensionless constant and S_p has been represented by the following dimensionless temperature stratification number s:

$$s=\frac{d\theta_a}{dy}=\frac{X_0}{\beta(T_0-T_{a,0})}S_p. \tag{20}$$

For a linearly stratified fluid, s is a constant. Hence, the dimensionless fountain height y_m has the following scaling relation with Fr, Re, and s:

$$y_m=\frac{Y_m}{X_0}\sim \mathrm{Fr}^{(1+c)} s^c \mathrm{Re}^{-d}. \tag{21}$$

For plane fountains, M_0, B_0, S_p, and ν have the following units:

$$M_0[=]L^3T^{-2}, \quad B_0[=]L^3T^{-3}, \quad S_p[=]L^{-1}, \quad \nu[=]L^2T^{-1}. \tag{22}$$

Then from Eq. (13), we have

$$L[=](L^3T^{-2})^a(L^3T^{-3})^b(L^{-1})^c(L^2T^{-1})^d [=]L^{(3a+3b-c+2d)}T^{(-2a-3b-d)}. \tag{23}$$

Hence, dimensional consistency then requires

$$3a+3b-c+2d=1, \tag{24}$$

$$-2a-3b-d=0, \tag{25}$$

which give the following relations:

$$a=1+c-d, \quad b=-\tfrac{1}{3}(2+2c-d). \tag{26}$$

With these relations, we find that for plane fountains

$$Y_m[=]2^{(1/3)(1+c-2d)}[\beta(T_0-T_{a,0})]^c \times \mathrm{Fr}^{(2/3)(2+2c-d)} s^c \mathrm{Re}^{-d} X_0 \sim \mathrm{Fr}^{(2/3)(2+2c-d)} s^c \mathrm{Re}^{-d} X_0, \tag{27}$$

and $2^{(1/3)(1+c-2d)}[\beta(T_0-T_{a,0})]^c$ is a dimensionless constant. Hence, the dimensionless fountain height y_m has the following scaling relation with Fr, Re, and s:

$$y_m=\frac{Y_m}{X_0}\sim \mathrm{Fr}^{(2/3)(2+2c-d)} s^c \mathrm{Re}^{-d}. \tag{28}$$

The powers c and d in Eqs. (21) and (28) remain unknown, however tentative values may be obtained from a scaling analysis as follows. The scaling analysis uses the quantities X_h and Y_h, where X_h is the distance, at which the fountain outflow has formed a viscous intrusion, and Y_h is the height of the intrusion. The analysis is based on the assumption that for low Reynolds number flow, the height of weak fountains is controlled by the rate, at which fluid can exit the fountain via the viscous intrusion that forms downstream of the fountain.

Over X_h, the primary balance in Eq. (7) will be between the horizontal pressure gradient and the vertical diffusion, giving

$$\frac{p^*}{x_h}\sim\frac{u^*}{\mathrm{Re}\, y_h^2}, \tag{29}$$

where $x_h=X_h/X_0$, $y_h=Y_h/X_0$, p^* is the dimensionless pressure scale, and u^* is the dimensionless horizontal velocity scale. Over the fountain height y_m, the pressure p^* is governed by the pressure-buoyancy balance, which, from Eq. (8), gives

$$\frac{p^*}{y_m^2}\sim\frac{s}{\mathrm{Fr}^2}, \tag{30}$$

where it is assumed that y_m and s are greater than 1.0, and thus the component of the pressure resulting from the stratification will dominate that resulting from the difference between the jet inlet density and the ambient density at the jet inlet.

Combining Eqs. (30) and (29) gives

$$\frac{y_m^2 s}{x_h}\sim\frac{u^*\mathrm{Fr}^2}{\mathrm{Re}\, y_h^2}. \tag{31}$$

Using Eq. (6) gives a scale for u^* in terms of a vertical velocity scale v^* as

$$u^*\sim\frac{x_h v^*}{y_m}, \tag{32}$$

which allows Eq. (31) to be written as

$$\frac{y_m^2 s}{x_h}\sim\frac{x_h v^*\mathrm{Fr}^2}{\mathrm{Re}\, y_m y_h^2}. \tag{33}$$

Using $v^*\sim 1$, this may be written as

$$y_m^3\sim\frac{x_h^2\mathrm{Fr}^2}{y_h^2\mathrm{Re}\, s}. \tag{34}$$

Assuming the intrusion height scales with the intrusion development distance, $y_h\sim x_h$ then gives

$$y_m\sim\frac{\mathrm{Fr}^{(2/3)}}{\mathrm{Re}^{(1/3)}s^{(1/3)}}. \tag{35}$$

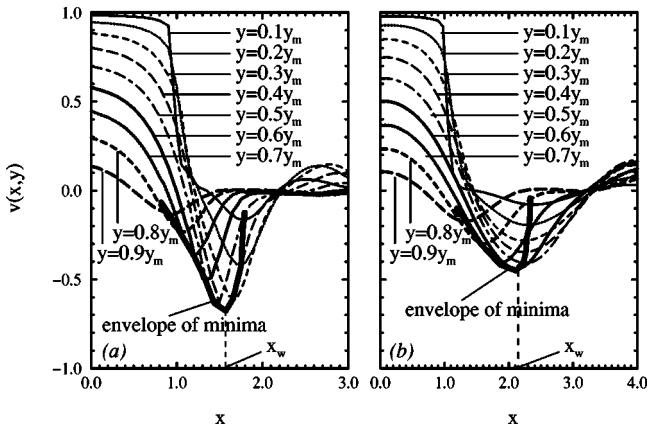

FIG. 2. Typical horizontal profiles of the vertical velocity at nine heights at a steady state for (a) an axisymmetric fountain and (b) a plane fountain, both with Fr=1.0, Re=200, Pr=1.0, and $s=2.5$.

On this basis, c may be tentatively set to $-1/3$ and d to 1/3 in the scaling relations Eqs. (21) and (28) for y_m.

2. Fountain width

As shown in the previous studies [16–19] when both a weak axisymmetric and a weak plane fountain flow in a homogeneous fluid are at a steady state, a characteristic fountain width X_w can be determined. This is also true for weak fountains in a stratified fluid. To show the definition of X_w, the horizontal profiles of the vertical velocity at $y=0.1y_m$, $0.2y_m$, $0.3y_m$, $0.4y_m$, $0.5y_m$, $0.6y_m$, $0.7y_m$, $0.8y_m$, and $0.9y_m$ at a steady state are presented in Fig. 2, obtained with the numerical simulation for both an axisymmetric and a plane fountain with Fr=1.0, Re=200, Pr=1, and $s=2.5$. At each height, it is seen that the vertical velocity $v(x,y)$, nondimensionalized by V_0, decreases gradually as x increases until at a specific x, $v(x,y)$ becomes 0 for each y, which is the location, at which the upflow terminates and the downflow begins. Beyond this location, $v(x,y)$ continues to reduce until a clearly defined minimum is reached, then increases until it again crosses the zero line. The envelope of the minima for each height itself has a clearly defined minimum as shown by the bold line in the figure, corresponding to $y=0.4y_m$ and $y=0.6y_m$ minimum, respectively, for the axisymmetric and plane fountains considered, which occur at $x\cong 1.57$ and 2.13, respectively. The minimum of the envelope is found to be clearly defined for all Fr used, similar to the previous studies of weak fountains in homogeneous fluids [17,18]. This width was defined to be the fountain width and was found to be the horizontal length scale that characterizes the fountain flow in a homogeneous fluid at a steady state [17,18].

As x_w is similar to y_m, the scalings obtained for y_m are also valid for x_w, that is, for axisymmetric fountains with Fr ≈ 1.0,

$$x_w = \frac{X_w}{X_0} \sim \mathrm{Fr}^{(1+c)} s^c \mathrm{Re}^{-d}, \tag{36}$$

where X_w is the dimensional fountain width, and for plane fountains with Fr ≈ 1.0,

$$x_w \sim \mathrm{Fr}^{(2/3)(2+2c-d)} s^c \mathrm{Re}^{-d}. \tag{37}$$

With $c=-1/3$ and $d=1/3$, these relations become

$$x_w \sim \frac{\mathrm{Fr}^{(2/3)}}{\mathrm{Re}^{(1/3)} s^{(1/3)}}, \tag{38}$$

3. Thickness of temperature layer

Similarly, M_0, B_0, and S_p are also important for the development of the temperature layer, together with the thermal diffusivity κ instead of ν. Following the same procedure as for y_m, we find that dimensional consistency gives

$$\Delta Y_T \sim X_0 \mathrm{Fr}^{(1+c)} s^c (\mathrm{Re\,Pr})^{-d}, \tag{39}$$

for axisymmetric fountains with Fr ≈ 1.0, which then gives the dimensionless temperature thickness Δy_T as

$$\Delta y_T = \frac{\Delta Y_T}{X_0} \sim \mathrm{Fr}^{(1+c)} s^c (\mathrm{Re\,Pr})^{-d}, \tag{40}$$

and for plane fountains with Fr ≈ 1.0,

$$\Delta y_T \sim \mathrm{Fr}^{(2/3)(2+2c-d)} s^c (\mathrm{Re\,Pr})^{-d}. \tag{41}$$

With $c=-1/3$ and $d=1/3$, these relations become

$$\Delta y_T \sim \frac{\mathrm{Fr}^{2/3}}{(\mathrm{Re\,Pr}\, s)^{1/3}}. \tag{42}$$

4. Time scales

There are two time scales t_{ms} and t_{mf} to represent, respectively, the time scale for the fountain flow in the fountain core, which is the domain enclosed by $x=x_w$ and $y=y_m$, to reach a steady state and the time scale for the full development of the temperature layer, defined as follows:

$$t_{ms} \sim \frac{Y_m}{V_m}, \quad t_{mf} \sim \frac{\Delta Y_T}{V_m}, \tag{43}$$

where V_m is the velocity that will scale with the development time.

For V_m, the governing parameters are M_0, B_0, ν, and S_p. A dimensional analysis similar to that used for y_m gives

$$V_m \sim V_0 \mathrm{Fr}^{-(1-c)} s^c \mathrm{Re}^{-d},$$

for axisymmetric fountains with Fr ≈ 1.0, and

$$V_m \sim V_0 \mathrm{Fr}^{-(1/3)(1-2c+d)} s^c \mathrm{Re}^{-d},$$

for plane fountains with Fr ≈ 1.0.

Hence,

$$t_{ms} \sim \frac{X_0}{V_0}\mathrm{Fr}^2, \quad t_{mf} \sim \frac{X_0}{V_0}\mathrm{Fr}^2\mathrm{Pr}^{-d}$$

for both axisymmetric and plane fountains with Fr ≈ 1.0, which give the following dimensionless time scales:

$$\tau_{ms} = \frac{t_{ms}}{(X_0/V_0)} \sim \mathrm{Fr}^2, \tag{44}$$

$$\tau_{mf} = \frac{t_{mf}}{(X_0/V_0)} \sim \mathrm{Fr}^2\mathrm{Pr}^{-d}. \tag{45}$$

With $d = -1/3$, Eq. (45) becomes

$$\tau_{mf} \sim \mathrm{Fr}^2\mathrm{Pr}^{-1/3}. \tag{46}$$

When $s = 0$, that is, in a homogeneous fluid, c must be equal to 0 and the scalings given above may be reworked to show that $d = 1/2$ and the scalings (21), (28), (36), (37), (40), (41), (44), and (45) reduce to

$$y_m \sim \mathrm{Fr}\,\mathrm{Re}^{-1/2}, \tag{47}$$

$$x_w \sim \mathrm{Fr}\,\mathrm{Re}^{-1/2}, \tag{48}$$

$$\Delta y_T \sim \mathrm{Fr}(\mathrm{Re}\,\mathrm{Pr})^{-1/2}, \tag{49}$$

$$\tau_{ms} \sim \mathrm{Fr}^2, \tag{50}$$

$$\tau_{mf} \sim \mathrm{Fr}^2 Pr^{-1/2}, \tag{51}$$

which are exactly the scaling relations obtained for weak fountains with Fr ≈ 1.0 in homogeneous fluids [17].

III. NUMERICAL RESULTS

A. Numerical method

The equations are discretized on a nonstaggered mesh using finite volumes, with standard second-order central differences used for the viscous, the pressure gradient and divergence terms. The QUICK third-order upwind scheme is used for the advective terms [21]. The momentum and temperature equations are solved using an ADI scheme. The second-order Adams-Bashforth scheme and Crank-Nicolson scheme are used for the time integration of the advective terms and the diffusive terms, respectively. To enforce the continuity, the pressure correction method is used to construct a Poisson's equation, which is solved using the preconditioned GMRES method. A detailed description of these schemes were given elsewhere [16,22] and the code has been used for the simulation of a range of buoyancy dominated flows [23,24].

Due to large variations in length scales, it is necessary to use a mesh that concentrates points in the fountain region and in the boundary layers and is relatively coarse in other regions. To construct such a mesh, a uniform fine mesh is used in the regions of $0 \leqslant x \leqslant 5$ and $0 \leqslant y \leqslant 2$ for axisymmetric fountains and of $0 \leqslant x \leqslant 4$ and $0 \leqslant y \leqslant 3$ for plane fountains, respectively, and a stretched mesh is distributed in the remaining regions both in the x and y direction. The meshes beyond the uniform mesh regions expand at a rate of 7.5% up to $x = 0.1(L/X_0 - 5)$ and $y = 0.1(H/X_0 - 2)$ for axisymmetric fountains and of 5% up to $x = 0.1(L/X_0 - 4)$ and $y = 0.1(H/X_0 - 3)$ for plane fountains, respectively. Beyond $x = 0.1(L/X_0 - 5)$ or $x = 0.1(L/X_0 - 4)$ and $y = 0.1(H/X_0 - 2)$ or $y = 0.1(H/X_0 - 3)$, the mesh size expansion rate decreases at a rate of 10% until it reaches 0, resulting in constant coarse meshes in the remaining regions.

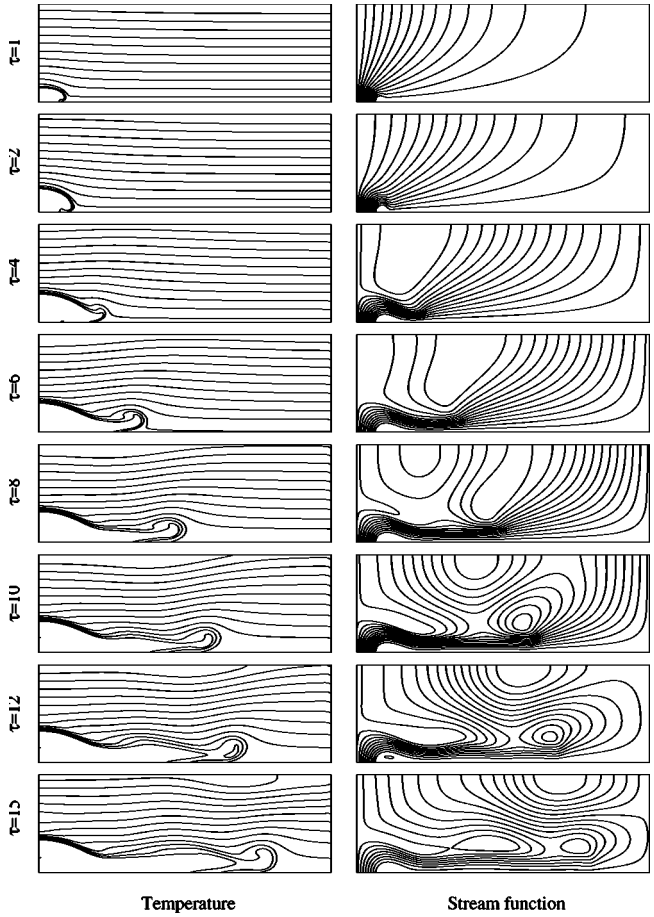

FIG. 3. Time evolution of numerically obtained temperature and stream function contours for a plane fountain with Fr = 1.0, Re = 200, Pr = 1.0, and $s = 2.5$.

B. Numerical validation of scaling relations

To provide an overview of the transient behavior of weak fountain flows in a stably stratified fluid, visualizations of the typical time evolution of the numerically simulated transient temperature and stream function contours are presented in Fig. 3 for a plane fountain with Fr = 1.0, Re = 200, Pr = 7, and $s = 2.5$. From initialization, the fountain is seen to grow in both height and breadth, producing a gravity intrusion that travels away from the fountain on the horizontal boundary. By the time $\tau = 10$, the fountain core has reaches full development, however the gravity intrusion continues to grow. Considerable work has been carried out on gravity intrusions and in a recent study, Maxworthy *et al.* [15] investigated the gravity intrusion produced by a lock flow in a stratified ambient. Although many of the features of that flow were dif-

ferent to the fountain flow considered here, the early stages of the intrusion flow are similar. Maxworthy *et al.* obtained intrusion nose propagation speeds for a range of domain height ratios, density differences, and stratifications. Applying their results to the fountain shown here predicts an intrusion nose velocity of ≈ 1.0. In Fig. 3 the intrusion nose has a velocity of 0.875 from $\tau=2$ to $\tau=4$, 1.0 from $\tau=4$ to $\tau=6$, 1.125 from $\tau=6$ to $\tau=8$, and 0.87 from $\tau=8$ to $\tau=10$, and these results are, therefore, in reasonable agreement with those of Maxworthy *et al.* [15].

It is found from this figure that the fundamental flow patterns are qualitatively similar to those of the weak fountains in homogeneous fluid with Fr$=1.0$, Re$=200$, and Pr$=7$ [17,18], although there are some distinct different features and quantitative differences which will be discussed below. The development of the axisymmetric fountain is qualitatively similar to that of the plane fountain, and for brevity, only the plane fountain has been shown.

To validate the scaling relations obtained in Sec. II, a series of numerical simulations have been carried out for both axisymmetric and plane fountains with selected values of the control parameters Fr, Re, Pr, and s. Specifically, Fr $=0.2$, 0.4, 0.6, 0.8, and 1.0 with Re$=200$, Pr$=1.0$, and $s=2.5$ are used to show the dependence of the scalings on Fr for axisymmetric fountains, whereas Fr$=0.2$, 0.4, 0.6, 0.8, and 1.0 with Re$=200$, Pr$=1.0$, and $s=3.0$ are used to show the dependence of the scalings on Fr for plane fountains; Re$=20$, 50, 100, and 200 with Fr$=1.0$, Pr$=1.0$, and $s=2.5$ are used to show the dependence of the scalings on Re for axisymmetric fountains, whereas Re$=20$, 50, 100, and 200 with Fr$=1.0$, Pr$=1.0$, and $s=3.0$ are used to show the dependence of the scalings on Re for plane fountains; Pr $=0.7$, 1.0, 4.0, 7.0, and 10.0 with Fr$=1.0$, Re$=200$, and $s=2.5$ are used to show the dependence of the scalings on Pr for axisymmetric fountains, whereas Pr$=0.7$, 1.0, 4.0, 7.0, and 10.0 with Fr$=1.0$, Re$=200$, and $s=3.0$ are used to show the dependence of the scalings on Pr for plane fountains; and $s=0.1$, 0.2, 0.3, 0.4, 0.5, 0.6, 1.0, 1.5, 2.0, 2.5, 3.0, 3.5, 4.0, 4.5, and 5.0 with Fr$=1.0$, Re$=200$, and Pr$=1.0$ are used to show the dependence of the scalings on s.

To use the numerical results to validate the scaling relations and to confirm that $-1/3$ is the appropriate value for the power c for weak fountains with Fr ≈ 1.0 and $s \geqslant 1.0$ in stratified fluids, we write the scaling relation for y_m in the following general form:

$$y_m = a + b s^c, \tag{52}$$

with fixed Re, Pr, and Fr, where $b=\mathrm{Fr}^{(1+c)}\mathrm{Re}^{-(1+c)/2}$ and a is included because the relation obtained for $s \approx 1.0$ may not extend unchanged to $s=0$ (as will be shown below). We then wish to plot Eq. (52) in log-log form, but we must transfer a to the left hand side of Eq. (52), giving

$$\ln(y_m - a) = b + c \ln(s), \tag{53}$$

and the slope of the log-log plot will then give c. However, the numerical results give a set of (y_m, s), they do not *a priori* give a. The procedure that was followed to determine c and a was to first plot $\ln(y_m)$ against $\ln(s)$, and obtain the slope of any linear region, providing a first estimate for c. This c was then used to obtain a, allowing $\ln(y_m - a)$ to be plotted against $\ln(s)$, giving a new estimate for c. This process was repeated until c was constant to three significant figures.

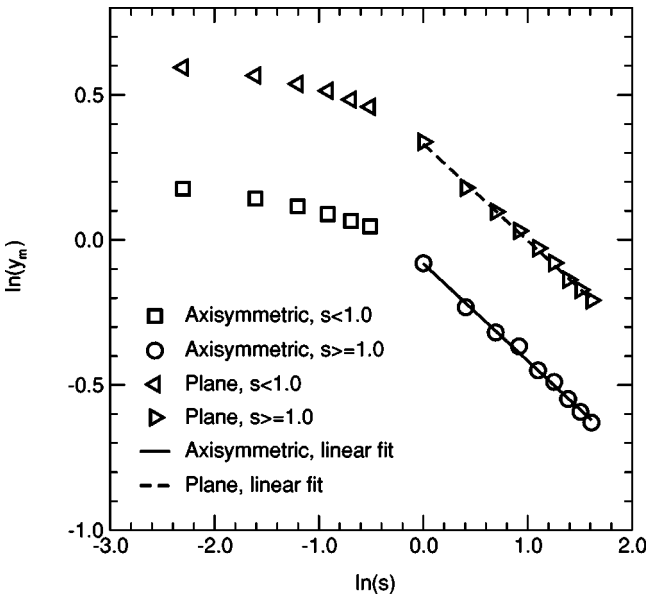

FIG. 4. $\ln(y_m)$ plotted against $\ln(s)$ for $1.0 \leqslant s \leqslant 5.0$ when Re $=200$, Fr$=1.0$, and Pr$=1.0$.

In Fig. 4, $\ln(y_m)$ is plotted against $\ln(s)$ for both axisymmetric and plane fountains with Re$=200$, Pr$=1.0$, and Fr $=1.0$. The linear fits in the region of $1.0 \leqslant s \leqslant 5.0$ give the value $c=-0.335(\pm 0.003)$ for both axisymmetric fountains and plane fountains. It is clear that $c=-1/3$ is the appropriate power for the scaling relation, Eqs. (21) and (28), as was obtained in the scaling analysis. The numerical results for $s<1.0$ do not show a linear relation between y_m and $s^{-1/3}$, indicating $c=-1/3$ is not the appropriate power for this range of s. In fact, as we discussed in Sec. II B 1, the scaling relation, Eq. (21), was obtained with the assumption that $s \geqslant 1.0$. For $s<1.0$, the slopes of the plots in Fig. 4 increase gradually towards 0, supporting the hypothesis that c must be 0 at $s=0$. Similar results for Re variation with s fixed show that for $s \geqslant 1$, $d \approx 1/3$, while for $s=0$, $d \approx 1/2$. In the subsequent numerical validations of the scaling relations, it has therefore been assumed that $c=-1/3$, $d=1/3$.

In Fig. 5, the numerical results validating the scaling relation for y_m [Eqs. (21) and (28)] are presented, where the four sets of data showing the respective dependence on Fr, Re, Pr, and s have been combined. The y_m have been plotted against Fr, Re, and s in the form $\mathrm{Fr}^{2/3}/(\mathrm{Re}\, s)^{1/3}$, as predicted by the scaling relation, no variation was observed with respect to Pr, again as predicted. The results are seen to then all collapse onto a single line for each of the axisymmetric and plane sets of data, confirming the scaling relations, which can be expressed in the following general linear quantitative relation for both axisymmetric and plane fountains in the ranges of Fr, Re, and s considered:

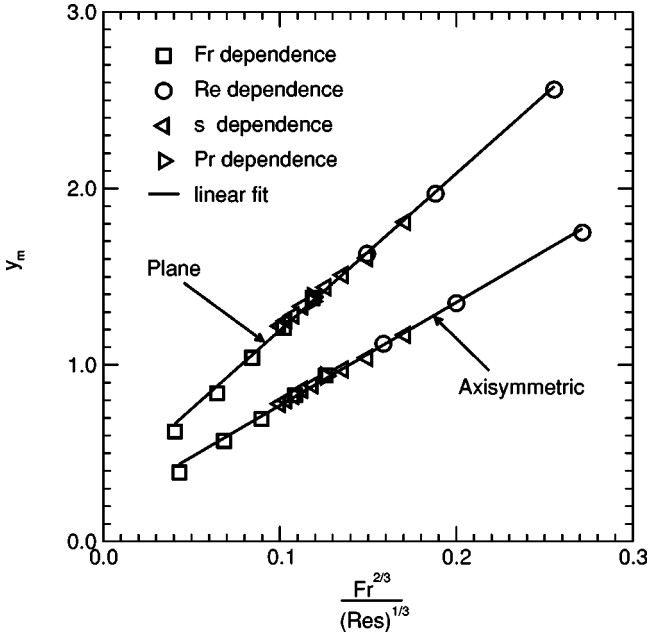

FIG. 5. y_m plotted against $\mathrm{Fr}^{2/3}/(\mathrm{Re}\,s)^{1/3}$.

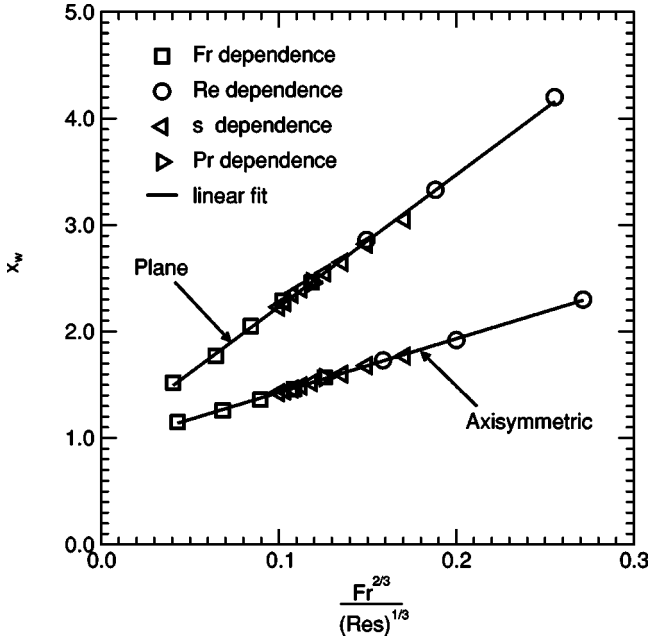

FIG. 6. x_w plotted against $\mathrm{Fr}^{2/3}/(\mathrm{Re}\,s)^{1/3}$.

$$y_m = a + b\frac{\mathrm{Fr}^{2/3}}{(\mathrm{Re}\,s)^{1/3}}, \tag{54}$$

where a and b are constants determined by regression of the numerical data, which are listed in Table I.

The numerical results validating the scaling relations for x_w [Eqs. (36) and (37)] are shown in Fig. 6. Once again, no Pr dependence was observed and so the data are plotted against $\mathrm{Fr}^{2/3}/(\mathrm{Re}\,s)^{1/3}$, as predicted by the scaling relation. The data collapse onto a line for each of the axisymmetric and plane fountain sets, with the linear regression coefficients given in Table I.

Results for the interface thickness, Δy_T, are shown in Fig. 7. In this case, the data were found to vary with Fr, Re, Pr, and s and have, therefore, been plotted against all these control parameters in the form $\mathrm{Fr}^{2/3}/(\mathrm{Re}\,\mathrm{Pr}\,s)^{1/3}$, again confirming the scaling prediction of Eqs. (40) and (41), with the linear regression coefficients given in Table I.

The times for the fountain core to reach a steady state, τ_{ms}, are shown in Fig. 8. In this case, the scaling relation, Eq. (44), shows variation with respect to Fr only, and the data have been plotted against Fr^2, with the linear behavior confirming the scaling prediction. The linear regression coefficients are shown in Table I. Results for the time to reach a steady state for the temperature layer, τ_{mf}, are shown in Fig. 9, plotted against $\mathrm{Fr}^2/\mathrm{Pr}^{1/3}$, again confirming the scaling relation, Eq. (45), with the linear regression coefficients shown in Table I.

The profiles of the vertical velocity $v(0,y)$ and temperature $\theta(0,y)$ characterize the fountain flow at a steady state [16–19]. To show the effect of Fr, Re, Pr, and s on $v(0,y)$, the numerical results are presented in Fig. 10 for six sets of Fr, Re, Pr, and s for both the axisymmetric and plane fountains. All sets of data fall onto a single curve, which is well approximated by

$$v(0,y) = 1.000 + 0.320\left(\frac{y}{y_m}\right) - 2.272\left(\frac{y}{y_m}\right)^2 + 0.952\left(\frac{y}{y_m}\right)^3 \tag{55}$$

TABLE I. Regression results for both axisymmetric and plane fountains.

y	x	Fountain type	a	b	R
y_m	$\mathrm{Fr}^{2/3}(\mathrm{Re}\,s)^{-1/3}$	Axisymmetric	0.186($\pm$0.012)	5.842($\pm$0.086)	0.9980
		Plane	0.306($\pm$0.015)	8.895($\pm$0.117)	0.9984
x_w	$\mathrm{Fr}^{2/3}(\mathrm{Re}\,s)^{-1/3}$	Axisymmetric	0.922($\pm$0.006)	5.056($\pm$0.102)	0.9992
		Plane	0.992($\pm$0.016)	12.401($\pm$0.126)	0.9991
Δy_T	$\mathrm{Fr}^{2/3}(\mathrm{Re}\,\mathrm{Pr}\,s)^{-1/3}$	Axisymmetric	0.023($\pm$0.002)	0.967($\pm$0.012)	0.9986
		Plane	0.019($\pm$0.002)	1.364($\pm$0.014)	0.9990
τ_{ms}	Fr^2	Axisymmetric	0.619($\pm$0.182)	8.248($\pm$0.198)	0.9943
		Plane	0.871($\pm$0.251)	14.887($\pm$0.273)	0.9967
τ_{mf}	$\mathrm{Fr}^2\mathrm{Pr}^{-1/3}$	Axisymmetric	0.673($\pm$0.107)	9.144($\pm$0.122)	0.9982
		Plane	1.021($\pm$0.191)	15.877($\pm$0.219)	0.9981

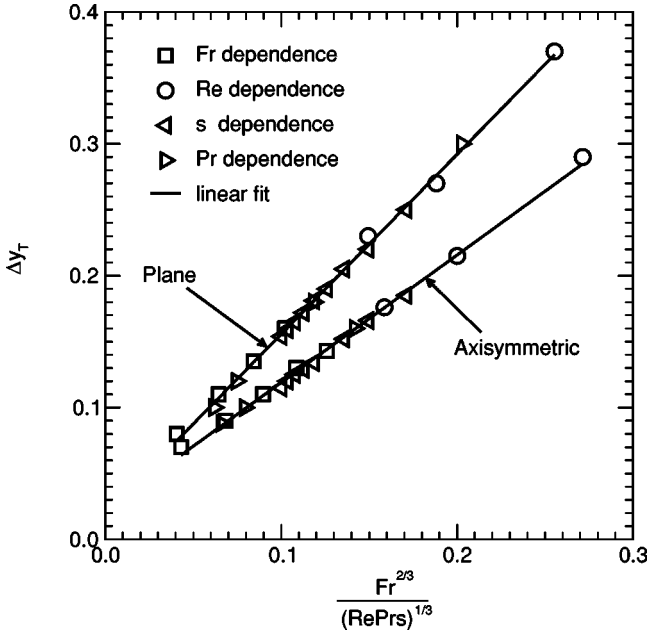

FIG. 7. Δy_T plotted against $\mathrm{Fr}^{2/3}/(\mathrm{Re\ Pr}\ s)^{1/3}$.

for the axisymmetric fountains and

$$v(0,y)=1.000+0.145\left(\frac{y}{y_m}\right)-2.287\left(\frac{y}{y_m}\right)^2+1.142\left(\frac{y}{y_m}\right)^3, \tag{56}$$

for the plane fountains, confirming that y_m is the appropriate length scale for $v(0,y)$, similar to that for weak fountains in homogeneous fluids [16–19].

In Fig. 11, the numerically obtained temperature profiles $\theta(0,y)$ on the symmetry axis are plotted against $(y-y_m)/\Delta y_T$ for the same sets of Fr, Re, Pr, and s as used in Fig. 10 for both the axisymmetric and plane fountains. All

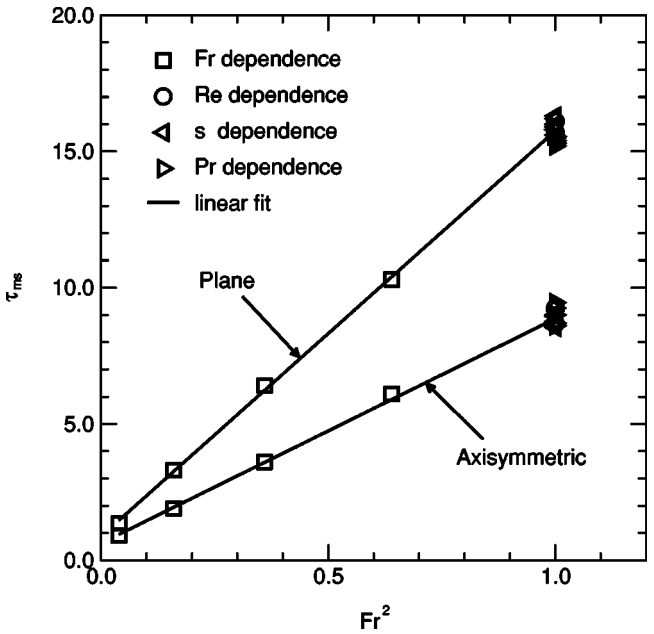

FIG. 8. τ_{ms} plotted against Fr^2.

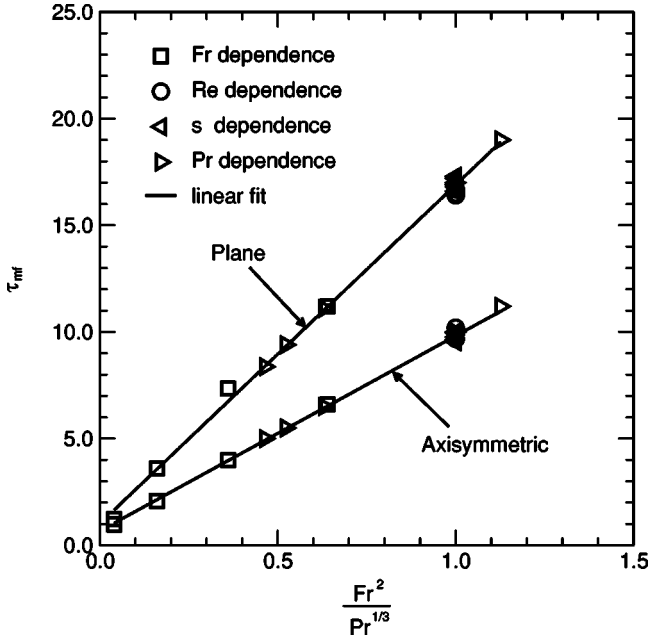

FIG. 9. τ_{mf} plotted against $\mathrm{Fr}^2/\mathrm{Pr}^{1/3}$.

sets of data again fall onto a single curve, indicating Δy_T and y_m are again the appropriate length scales for $\theta(0,y)$, that is,

$$\theta(0,y)\sim f\left(\frac{y-y_m}{\Delta y_T}\right), \tag{57}$$

similar to that for weak fountains in homogeneous fluids [16–19].

IV. CONCLUSIONS

The behavior of both weak axisymmetric and plane fountains that result from the injection of denser fluids upwards

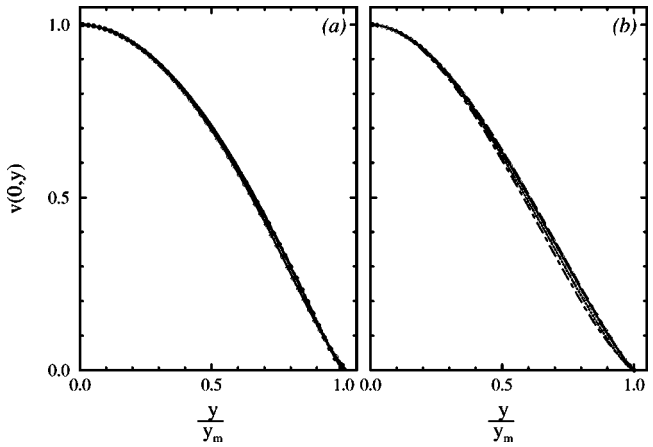

FIG. 10. Numerical simulated $v(0,y)$ plotted against y/y_m in the fountain core for six sets of Fr, Re, Pr, and s for (a) axisymmetric fountains and (b) plane fountains: ——, Fr=0.4, Re=200, Pr=1.0, s=2.5; · · · ·, Fr=1.0, Re=200, Pr=1.0, s=1.0; — - — -, Fr=1.0, Re=200, Pr=1.0, s=2.5; — · — · — · —, Fr=1.0, Re=200, Pr=1.0, s=5.0; ——○——, Fr=1.0, Re=50, Pr=1.0, s=2.5; ——●——, Fr=1.0, Re=200, Pr=7.0, s=2.5.

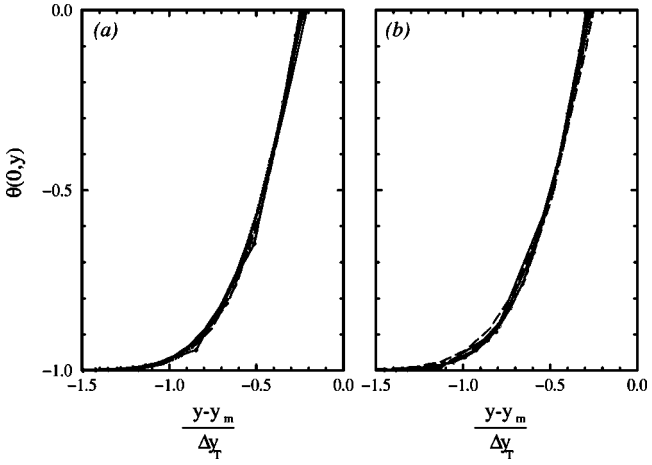

FIG. 11. Numerical simulated $\theta(0,y)$ plotted against $(y-y_m)/\Delta y_T$ in the fountain core for six sets of Fr, Re, Pr, and s for (a) axisymmetric fountains and (b) plane fountains: ——, Fr=0.4, Re=200, Pr=1.0, $s=2.5$; · · · ·, Fr=1.0, Re=200, Pr=1.0, $s=1.0$; — - — -, Fr=1.0, Re=200, Pr=1.0, $s=2.5$; — · — · — · —, Fr=1.0, Re=200, Pr=1.0, $s=5.0$; ——○——, Fr=1.0, Re=50, Pr=1.0, $s=2.5$; ——●——, Fr=1.0, Re=200, Pr=7.0, $s=2.5$.

into large containers containing stably stratified fluids has been studied using dimensional analysis, scaling analysis, and direct simulation with a time-accurate finite volume code.

For Fr ≈ 1.0, the specific momentum flux and specific buoyancy flux at the fountain discharge source are important control parameters. Additional control parameters are the stratification numbers of the ambient fluid and the viscosity of the fluid. Dimensional consistency provided scaling relations for y_m, x_w, Δy_T, τ_{ms}, and τ_{mf} which depended on the control parameters, together with the powers c and d. A scaling analysis, based on the assumption that the fountain height is controlled by the rate, at which fluid can exit the fountain via the downstream viscous intrusion, gave tentative values of $c=-1/3$, $d=1/3$. A series of numerical simulations show that the numerical results agree well with the analytical scaling relations and confirm that $c\cong -1/3, d\cong 1/3$ are the appropriate powers for both weak axisymmetric and plane fountains when $0.2\leqslant \mathrm{Fr}\leqslant 1.0$, $5\leqslant \mathrm{Re}\leqslant 500$, $0.7\leqslant \mathrm{Pr}\leqslant 10$, and $1.0\leqslant s\leqslant 5.0$. The numerical results also show that y_m and $(y-y_m)/\Delta y_T$ are the appropriate length scales for the profiles of vertical velocity and temperature on the symmetry axis for both axisymmetric and plane fountains in stratified fluids, similar to those for weak fountains in homogeneous fluids.

ACKNOWLEDGMENTS

The financial support from the National Natural Science Foundation (Grant No. 19872059) and the Yunnan Province of People's Republic of China to W. Lin and from the Australian Research Council are gratefully acknowledged.

[1] B.R. Morton, J. Fluid Mech. **5**, 151 (1959); B.R. Morton, Int. J. Air Poll. **1**, 184 (1959).
[2] J.S. Turner, J. Fluid Mech. **26**, 779 (1966); **173**, 431 (1986).
[3] G. Abraham, J. Hydraul. Res. **5**, 235 (1967).
[4] J.S. Turner, *Buoyancy Effects in Fluids* (Cambridge University Press, Cambridge, London, 1973).
[5] R.A. Seban, M.M. Behnia, and K.E. Abreau, Int. J. Heat Mass Transf. **21**, 1453 (1978).
[6] H.B. Fischer *et al.*, *Mixing in Inland and Coastal Waters* (Academic, New York, 1979).
[7] C.J. Chen and W. Rodi, *Vertical Turbulent Buoyant Jets* (Pergamon, Oxford, New York, 1980); W. Rodi, *Turbulent Buoyant Jets and Plumes* (Pergamon, Oxford, New York, 1982).
[8] E.J. List, Annu. Rev. Fluid Mech. **14**, 189 (1982).
[9] T. Mizushina, F. Ogino, H. Takeuchi, and H. Ikawa, Wärme-Stoffübertrag **16**, 235 (1982).
[10] I.H. Campbell and J.S. Turner, J. Petrol. **30**, 885 (1989).
[11] W.D. Baines, J.S. Turner, and I.H. Campbell, J. Fluid Mech. **212**, 557 (1990); W.D. Baines, A.F. Corriveau, and T.J. Reedman, *ibid.* **255**, 621 (1991).
[12] L.J. Bloomfield and R.C. Kerr, J. Fluid Mech. **358**, 335 (1998); L.J. Bloomfield and R.C. Kerr, *ibid.* **389**, 27 (1999); L.J. Bloomfield and R.C. Kerr, *ibid.* **424**, 197 (2000).
[13] J.E. Simpson, *Gravity Currents in the Environment and the Laboratory* (Cambridge University Press, Cambridge, London, 1997).
[14] T. Maxworthy, Annu. Rev. Fluid Mech. **29**, 327 (1997).
[15] T. Maxworthy, J. Leilich, J.E. Simpson, and E.H. Meiburg, J. Fluid Mech. **453**, 371 (2002).
[16] W. Lin, Ph.D. thesis, The University of Sydney, Sydney, 2000 (unpublished).
[17] W. Lin and S.W. Armfield, J. Fluid Mech. **403**, 67 (2000).
[18] W. Lin and S.W. Armfield, Int. J. Heat Mass Transf. **43**, 3013 (2000).
[19] W. Lin and S.W. Armfield, Numer. Heat Transfer, Part A **38**, 377 (2000).
[20] J.A. Duffie and W.A. Beckman, *Solar Engineering of Thermal Processes* (Wiley, New York, 1991).
[21] B.P. Leonard, Comput. Methods Appl. Mech. Eng. **19**, 59 (1979).
[22] S.W. Armfield, Comput. Fluids **20**, 1 (1991); S.W. Armfield, J. Comput. Phys. **114**, 176 (1994); S.W. Armfield and R. Street, *ibid.* **153**, 660 (1999).
[23] J.C. Patterson and S.W. Armfield, J. Fluid Mech. **219**, 469 (1990); S.W. Armfield and J.C. Patterson, *ibid.* **239**, 195 (1992); S.W. Armfield and W. Debler, Int. J. Heat Mass Transf. **36**, 519 (1993); S.W. Armfield and R. Janssen, Int. J. Heat Fluid Flow **17**, 539 (1996); A. Javam, J. Imberger, and S.W. Armfield, J. Fluid Mech. **396**, 183 (1999).
[24] W. Lin and S.W. Armfield, Energy **23**, 719 (1998); Int. J. Heat Mass Transf. **42**, 4117 (1999); Int. J. Heat Fluid Flow **22**, 72 (2001); W. Lin, S.W. Armfield, and P.L. Morgan, Int. J. Heat Mass Transf. **45**, 451 (2002).